Frequency-domain optimization of fixed-structure controllers

van Solingen, E.; van Wingerden, J. W.; Oomen, T.

DOI
10.1002/rnc.3699

Publication date
2016

Document Version
Final published version

Published in
International Journal of Robust and Nonlinear Control

INTERNATIONAL JOURNAL OF ROBUST AND NONLINEAR CONTROL
Int. J. Robust Nonlinear Control (2016)
Published online in Wiley Online Library (wileyonlinelibrary.com). DOI: 10.1002/rnc.3699

Frequency-domain optimization of fixed-structure controllers

E. van Solingen[1], J.W. van Wingerden[1,*,†] and T. Oomen[2]

[1]*Delft Center for Systems and Control, Faculty of Mechanical, Maritime and Materials Engineering, Delft University of Technology, Delft 2628 CD, The Netherlands*
[2]*Eindhoven University of Technology, Department of Mechanical Engineering, Control Systems Technology Group, Eindhoven 5600 MB, The Netherlands*

SUMMARY

This paper aims to introduce a new approach to optimize the tunable controller parameters of linear parameterizable controllers. The presented approach is frequency-domain based and can therefore directly be used to tune, among others, proportional integral derivative controllers, low/high-pass filters, and notch filters, using a Frequency Response Function of the plant. The approach taken in this paper is to extract the tunable controller parameters into a diagonal matrix gain and absorb the remainder of the controller in the plant. Then, the generalized Nyquist stability criterion is exploited so as to impose stability and $\mathcal{H}_\infty$ performance specifications on the closed-loop system. It is shown that the approach results in a convex feasibility problem for certain controller cases and can be reformulated such that it can also be used for grey-box system identification. Simulation and experimental examples demonstrate the efficacy of the approach. © 2016 The Authors. *International Journal of Robust and Nonlinear Control* published by John Wiley & Sons, Ltd.

Received 2 October 2015; Revised 9 August 2016; Accepted 4 October 2016

KEY WORDS: frequency-domain $\mathcal{H}_\infty$ controller design; fixed-structure control; decentralized control; grey-box system identification; Nyquist stability criterion

1. INTRODUCTION

Many systems can be modeled accurately by means of first-principle models, but will never exactly match the real-world system because of, for instance, manufacturing errors and imperfections [1]. Consequently, a controller designed based upon the first-principles model is likely to not give maximum performance when implemented. Hence, a controller based on data, that is, obtained through system identification, is likely to result in better control performance. In particular for lightly damped high-order systems, obtaining accurate models from data can be cumbersome. Instead, a highly accurate non-parametric Frequency Response Function (FRF) can directly be obtained [2]. Direct control design based on the FRF may avoid the difficulties associated with parametric modeling.

Besides the importance of designing the controller based on an accurate model, the use of controllers with pre-specified structure is important. First, these are directly retunable when implementing in the field, which is in sharp contrast to classical optimal and robust control design techniques that lead to high-order controllers (e.g., as high as the order of the plant [3, 4]). Second, industrial controllers often are implemented in dedicated hardware, directly imposing constraints on the controller structure. Because both the controller structure and order are fixed *a priori*, only the

*Correspondence to: J.W. van Wingerden, Delft Center for Systems and Control, Faculty of Mechanical, Maritime and Materials Engineering, Delft University of Technology, Mekelweg 2, Delft 2628 CD, The Netherlands.
†E-mail: j.w.vanwingerden@tudelft.nl

tunable parameters need to be found such that the performance specifications are met. Unlike well-known solutions to unstructured control synthesis problems (e.g., using Riccati equations [5] or linear matrix inequality techniques [6, 7]), the main problem that arises when imposing constraints on the controller structure is that the resulting optimization problem is no longer convex and is in general considered to be NP-hard [8–10].

In this paper, we develop a control design approach that takes the following requirements into account. First, the structure and order of the controller are specified *a priori* and, hence, the method should be able to deal with this type of controllers. Second, the method should be able to handle both SISO and MIMO controllers. Third, the method should be able to design the controllers based on an FRF of the plant. Finally, approximations of the involved controller optimizations are regarded as undesired.

In the past decades, fixed-structure control synthesis has received considerable attention. In the context of iterative linear matrix inequality solutions, such approaches have been developed in [11–14]. Typically, these methods enable the controller synthesis for very specific controller structures or introduce conservatism. Related results where the order of the controller is specified are presented in [15] where sum-of-squares techniques for fixed-order $\mathcal{H}_\infty$ controller synthesis are used, in [16] where positive polynomials for the same objective are used, and in [17] where evolutionary algorithms are used to design low-order controllers. Furthermore, a convex-concave optimization procedure for proportional integral derivative (PID) controller design is outlined in [18], randomized algorithms are used in [19, 20], a surrogate convex upper bound on the $\mathcal{H}_\infty$ norm is used in [21], and an alternative for the Youla parameterization in [22]. Non-smooth optimization techniques are used in [23–26], which are implemented in the MATLAB Robust Control Toolbox. All the aforementioned methods are limited by being only applicable to PID control, SISO systems, or cannot be applied to FRFs.

A structured controller design method using frequency-domain data is found in [27], where pre-defined fixed-structure controllers are optimized with respect to closed-loop performance specifications based on FRF data of the plant. A robust controller design method for a class of uncertainties using frequency-domain data is presented in [28]. In [29], a subset of stabilizing fixed-order controllers using a set of linear inequalities is calculated from the frequency response of the plant. The fixed-order controllers achieve some $\mathcal{H}_\infty$ norms on the (complementary) sensitivity function. The latter work is an extension to the work of [30], in which a complete set of stabilizing PID controllers is calculated directly from the plant FRF. The latter model-free-based and frequency-domain-based design methods require either approximation, or can only handle first-order or fixed-order controllers.

In [31, 32], it is shown that the $\mathcal{H}_\infty$ robust performance condition can be represented in the Nyquist diagram by constraints with respect to the tunable parameters of linearly parameterizable controllers. The constraints are convexified by using a desired open-loop transfer function (which is an approximation of the open-loop transfer function). The method [32] can be applied to SISO systems and is extended in [31] to include MIMO systems. The MIMO case is shown to work well when the open-loop transfer function can be made diagonally dominant by the controller, which does not exploit the full potential of centralized multivariable control.

The aim of this paper is to develop a frequency-domain approach for $\mathcal{H}_\infty$ fixed-structure controller design and grey-box system identification. The methodology can directly use a measured FRF obtained from the plant to compute the tunable parameters of linearly parameterizable SISO and MIMO controllers. Performance specifications of the closed-loop system are imposed by weights on the (complementary) sensitivity function(s) in the frequency-domain. The methodology presented in this paper exploits the generalized Nyquist stability criterion and satisfies, by constraining the Nyquist curve from certain parts of the Nyquist diagram, stability and performance requirements of the closed-loop system. It is shown that for special control cases, the controller design results in a convex feasibility problem, but will generally result in a feasibility problem that is multilinear in the tunable controller parameters. It is shown that the methodology can also be directly used for grey-box system identification.

The proposed approach can also be used for integrating the design of plant and controller. Similarly to extracting the tunable parameters of the controller, structural parameters of plant need to be

DOI: 10.1002/rnc

extracted into a diagonal form. Thus, the diagonal controller structure is extended with structural-related parameters. The inclusion of tunable structural parameters does not change the methodology. The property to simultaneously design plant and controller is appealing, because it can lead to more efficient designs (e.g., [33–38]).

To summarize, the main contributions of this paper are

- Fixed-structure $\mathcal{H}_\infty$ controller design based on an FRF of the plant;
- Grey-box system identification method based on an FRF of the plant.

Preliminary results have been published in [39, 40]. This paper extends these results with theoretical and experimental results, including a special controller case resulting in the controller tuning becoming a convex feasibility problem.

The results in [31, 32] resemble the approach in our paper. Two important differences are the following. First, the approach in this paper does not rely on any approximation, in contrast to the method in [32], in which the open-loop transfer function is approximated by a user-defined desired open-loop transfer function. The approach presented here requires the designer to introduce line constraints in the Nyquist diagram. Second, the method in this paper naturally extends to multivariable controller design, whereas in [31], MIMO controller design is carried out such that the diagonal elements achieve single-loop performance specifications and the off-diagonal elements principally decouple the system.

The paper is organized as follows. In Section 2, the general problem formulation is outlined. The method to tune the parameters of fixed-structure controllers along with some practical aspects is subsequently presented in Section 3. The extension of the method to a grey-box system identification method is given in Section 4. Section 5 presents the experimental setup. The methods are demonstrated in Section 6 through a simulation study and the experimental setup. The paper is concluded in Section 7.

2. PROBLEM FORMULATION

In this section, the $\mathcal{H}_\infty$ control design problem is defined, the class of controllers including several examples is described, and stability and performance of the closed-loop system are defined.

2.1. Problem statement

The following partitioning of the generalized plant, in which a part of the controller will be absorbed, is considered

$$\begin{bmatrix} z \\ y \end{bmatrix} = \underbrace{\begin{bmatrix} P_{11}(s) & P_{12}(s) \\ P_{21}(s) & P_{22}(s) \end{bmatrix}}_{P(s)} \begin{bmatrix} w \\ u \end{bmatrix}, \tag{1}$$

with $z \in \mathbb{R}^{n_z}$, $w \in \mathbb{R}^{n_w}$, $y \in \mathbb{R}^{n_m}$, and $u \in \mathbb{R}^{n_m}$. The transfer functions $P_{11}(s)$, $P_{12}(s)$, $P_{21}(s)$, and $P_{22}(s)$ have corresponding dimensions and are all assumed to be stable.[‡] The controller parameters are real scalars, that is, $\phi \in \mathbb{R}^{n_m}$. With these definitions, the controller is defined as

$$u = \underbrace{\begin{bmatrix} \phi_1 & & 0 \\ & \ddots & \\ 0 & & \phi_m \end{bmatrix}}_{K} y. \tag{2}$$

and the closed-loop system is obtained by

$$T_{wz}(s) = F_l(P, K) = P_{11} + P_{12}K(I - P_{22}K)^{-1}P_{21},$$

[‡]In this paper, only stable generalized plants are considered; however, the method can be extended to include unstable generalized plants.

DOI: 10.1002/rnc

where F_l denotes the lower linear fractional transformation (LFT). The goal is to find the controller parameters ϕ that achieve $||T_{wz}(s)||_\infty < 1$ (the reason for this objective will become clear in Section 2.3).

Note that for a freely parameterized controller K, this problem is convex [3], but typically leads to a solution having the same order as the generalized plant, which is typically not desired in practical applications. For a fixed-structure controller, the problem is no longer guaranteed to be convex.

2.2. Linear parameterizable controllers

The plant and controller structure as defined in (1) and (2) for a PID controller can be obtained as follows. Let a PID controller be given by

$$K_{\text{PID}}(s) = K_p + \frac{K_i}{s} + \frac{K_d s}{T_f s + 1}, \tag{3}$$

then a diagonal structure with the controller parameters $\phi_{\text{PID}} = [K_p \; K_d \; K_i]$ as in Figure 1 is obtained in a straightforward manner (negative feedback is assumed). If desired, the time constant T_f can also be pulled out of the structure.

More generally, the diagonal controller structure as described precedingly can be obtained from more generic parameterizations. That is, any well-posed rational function $R(b)$ can be written as an LFT [41]

$$R(b) = F_l(M, b \otimes I), \tag{4}$$

with M a fixed matrix and $b \otimes I$ a diagonal matrix containing the parameters that define the rational function $R(b)$ (see [25] and [42] for examples). Note that repeated copies of the parameters b may arise, which change the type of optimization problem that is discussed in the next section.

A more general linear controller parameterization (including (3)) can be obtained with the use of basis functions [43]. In [32, 44], Laguerre basis functions

$$\chi_i(s) = \frac{\sqrt{2\xi}(s-\xi)^{(i-1)})}{(s+\xi)^i} \quad \text{for } i \geqslant 1,\ \xi > 0,\ \chi_0(s) = 1 \tag{5}$$

are used. By multiplying each basis function with a scalar, for example, $\phi_{\text{B}} = [\phi_i, \ldots, \phi_m]^T \chi$, any stable rational finite order transfer function can be approximated (for a sufficient number of basis functions). The Laguerre basis functions can be incorporated by absorbing the basis functions into the generalized plant and creating a diagonal structure similar to Figure 1 with the elements of ϕ_{B} on the diagonal. The tuning parameter ξ and the number of bases i need to be selected beforehand, for which a practical guideline to select the basis functions is given in [32].

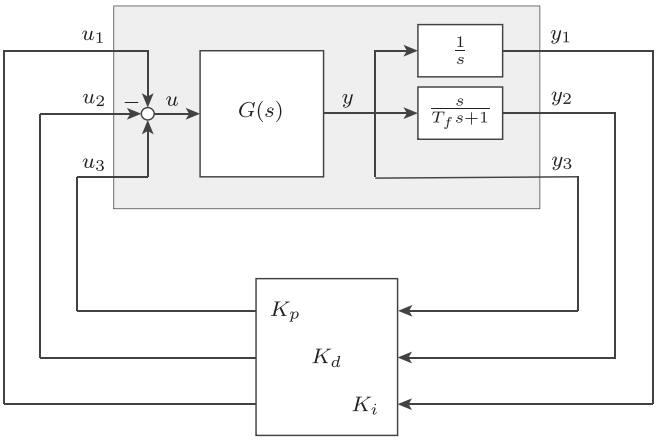

Figure 1. Linear parameterization of a proportional integral derivative controller. The generalized plant is indicated by the grey box.

DOI: 10.1002/rnc

2.3. Stability and performance

In order to compute the controller parameters ϕ that result in $\|T_{wz}(s)\|_\infty < 1$, consider the following approach, assuming a stable generalized plant $P(s)$ and given the frequency response data of $P(s)$ denoted by $P(j\omega)$. By making use of the generalized Nyquist stability criterion of [45], two definitions are formulated.

Definition 1 (Stability [4]*)*
The closed-loop system T_{wz} in Figure 2 is asymptotically stable if for a given stable generalized plant $P(j\omega)$, the Nyquist plot of

$$\det\left(I - \begin{bmatrix} \phi_1 & & 0 \\ & \ddots & \\ 0 & & \phi_m \end{bmatrix} P_{22}(j\omega)\right), \quad \forall\omega, \tag{6}$$

does not encircle the origin.

This is the generalized Nyquist theorem for a positive feedback system with stable loop transfer function $KP_{22}(j\omega)$.

Definition 2 (Performance [4]*)*
The closed-loop system $\|T_{wz}\|_\infty$ in Figure 3 satisfies the performance requirement $||T_{wz}||_\infty < 1$, if for a given stable generalized plant $P(j\omega)$, the Nyquist plot of

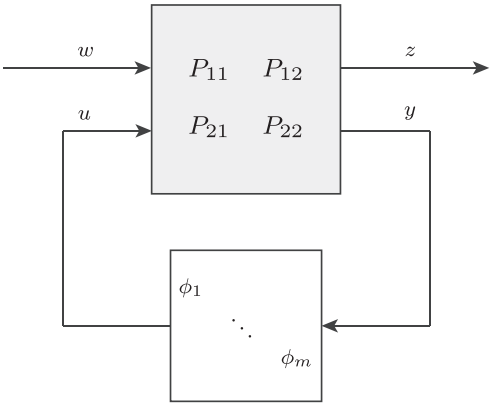

Figure 2. Generalized plant with linear parameterized controller.

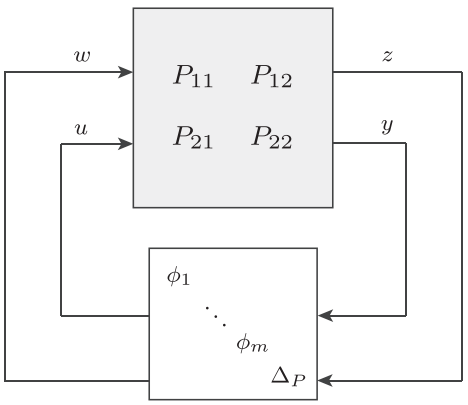

Figure 3. Closed-loop system including performance $\Delta_P(s)$

DOI: 10.1002/rnc

$$\det\left(I - \left[\begin{array}{c|ccc} \Delta_P(j\omega) & 0 & & \\ \hline & \phi_1 & & 0 \\ 0 & & \ddots & \\ & 0 & & \phi_m \end{array}\right] P(j\omega)\right), \ \forall\omega, \forall\Delta_P(j\omega), \tag{7}$$

does not encircle the origin for any stable rational transfer function $\Delta_P \in \mathcal{RH}_\infty^{n_w \times n_z}$ and $\|\Delta_P(s)\|_\infty \leqslant 1$.

Note that the system in Figure 3 is obtained by including, in Figure 2, a full complex 'perturbation' block $\Delta_P(j\omega)$ in feedback with the exogenous input w and exogenous output z. The 'perturbation' should be regarded as fictitious as it is only used as a means to examine the performance specification and is thus not a physical perturbation. The proof of (7) follows along the lines of [4, Theorem 8.7 and the proofs thereof]. In the remainder of this paper, we refer to *stability* and *performance* as defined in (6) and (7).

Further note that intergrid errors are not within the scope of this paper and we therefore assume a sufficiently dense frequency grid. The interested reader is referred to [46] for a discussion on the density of the frequency grid.

3. NYQUIST-BASED CONTROLLER DESIGN

The procedure to compute the controller parameters such that the closed-loop system is stable and $\|T_{wz}\|_\infty < 1$ is outlined in this section. The first step is to analyze the relation between the determinant expression and the controller parameters. The constraints preventing the Nyquist curve from encircling the origin are subsequently introduced. Then, relevant constraints are obtained by realizing the performance perturbation block Δ_P with maximum singular value. Finally, a feasibility problem is obtained from the imposed line constraints and the realization of Δ_P, and it is shown that in certain controller cases this feasibility problem is in fact convex in the controller parameters.

3.1. Determinant for stability and performance

In this paragraph, the determinant expressions are explored to show the dependence on the controller parameters ϕ. The determinant expression for two controller parameters (i.e., $\phi \in \mathbb{R}^2$) for closed-loop stability (6) is given by

$$Q(\phi, j\omega) = 1 - P_{22}^{(11)}\phi_1 - P_{22}^{(22)}\phi_2 + \left(P_{22}^{(11)}P_{22}^{(22)} - P_{22}^{(12)}P_{22}^{(21)}\right)\phi_1\phi_2, \tag{8}$$

for which the following partitioning of $P_{22}(j\omega)$ is considered

$$P_{22}(j\omega) = \left[\begin{array}{cc} P_{22}^{(11)}(j\omega) & P_{22}^{(12)}(j\omega) \\ P_{22}^{(21)}(j\omega) & P_{22}^{(22)}(j\omega) \end{array}\right].$$

Similarly, the determinant expression for two controller parameters, a single exogenous input w, and exogenous output z for closed-loop performance (7) is given by

$$\begin{aligned} Q_\Delta(\phi, j\omega) = 1 &- P_{11}\Delta_P + \left(P_{11}P_{22}^{(11)}\Delta_P - P_{12}^{(11)}P_{21}^{(11)}\Delta_P - P_{22}^{(11)}\right)\phi_1 \\ &+ \left(P_{11}P_{22}^{(22)}\Delta_P - P_{12}^{(12)}P_{21}^{(21)}\Delta_P - P_{22}^{(22)}\right)\phi_2 \\ &+ \Bigg(P_{22}^{(11)}P_{22}^{(22)} - P_{22}^{(12)}P_{22}^{(21)} - P_{11}P_{22}^{(11)}P_{22}^{(22)}\Delta_P \\ &+ P_{11}P_{22}^{(12)}P_{22}^{(21)}\Delta_P + P_{12}^{(11)}P_{21}^{(11)}P_{22}^{(22)}\Delta_P \\ &+ P_{12}^{(11)}P_{22}^{(12)}P_{21}^{(21)}\Delta_P - P_{12}^{(12)}P_{21}^{(11)}P_{22}^{(21)}\Delta_P + P_{12}^{(12)}P_{22}^{(11)}P_{21}^{(21)}\Delta_P\Bigg)\phi_1\phi_2, \end{aligned} \tag{9}$$

DOI: 10.1002/rnc

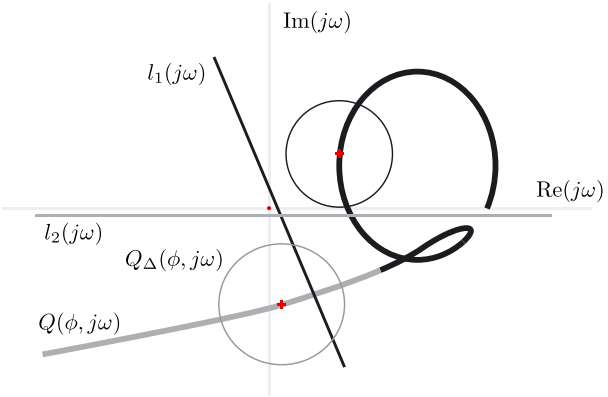

Figure 4. Nyquist diagram for $Q(\phi, j\omega)$ (stability) and $Q_\Delta(\phi, j\omega)$ (performance). The colors indicate which of the constraints $l_1(j\omega)$ and $l_2(j\omega)$ hold for which part of the Nyquist plots.

for which the following partitioning of the generalized plant $P(j\omega)$ is considered

$$P(j\omega) = \begin{bmatrix} P_{11}(j\omega) & P_{12}^{(11)}(j\omega) & P_{12}^{(12)}(j\omega) \\ P_{21}^{(11)}(j\omega) & P_{22}^{(11)}(j\omega) & P_{22}^{(12)}(j\omega) \\ P_{21}^{(21)}(j\omega) & P_{22}^{(21)}(j\omega) & P_{22}^{(22)}(j\omega) \end{bmatrix}.$$

From the determinant expressions in (8) (for stability) and (9) (for performance), it can be seen that the expressions are bilinear in ϕ and multilinear[§] for more parameters. In the next sections, the determinant expressions (8)–(9) are constrained in order to satisfy the Nyquist criterion.

3.2. Constraints in the Nyquist diagram

The main idea in the proposed Nyquist-based approach is to constrain the Nyquist curves from encircling or crossing the origin. Consider the Nyquist curves of (6) and (7), respectively denoted as $Q(\phi, j\omega)$ and $Q_\Delta(\phi, j\omega)$, for a certain generalized plant $P(j\omega)$ and a parameter vector ϕ, illustrated in Figure 4. It is well known that the thick solid line represents the Nyquist curve $Q(\phi, j\omega)$ (obtained with (8)) and the discs forming a banded graph with centers at the solid line represent the Nyquist curve $Q_\Delta(\phi, j\omega)$ (obtained with (7)).

The closed-loop system T_{wz} is stable if and only if the Nyquist curve $Q(\phi, j\omega)$ does not encircle the origin. Moreover, performance is achieved if and only if the Nyquist curve $Q_\Delta(\phi, j\omega)$ does not encircle the origin. The latter two definitions impose clear constraints on the Nyquist curve. Hence, considering Figure 4 in this context, the lines $l_1(j\omega)$ and $l_2(j\omega)$ constrain the Nyquist curve from encircling the origin. Note the different colors of the Nyquist curves $Q(\phi, j\omega)$ and $Q_\Delta(\phi, j\omega)$, and the constraint lines $l_1(j\omega)$ and $l_2(j\omega)$, illustrating the relation and frequency dependency of the constraint lines and the Nyquist curves. Further note that constraining the Nyquist curve by lines was earlier proposed in [47, 48].

The lines $l_1(j\omega)$ and $l_2(j\omega)$ can be introduced as following. To constrain the Nyquist curve $Q(\phi, j\omega)$ above the line $l_1(j\omega)$ in Figure 4, it should hold that

$$\mathrm{Im}(Q(\phi, j\omega)) > \alpha_1 \mathrm{Re}(Q(\phi, j\omega)) + c_1, \tag{10}$$

where $\mathrm{Re}(\cdot)$ and $\mathrm{Im}(\cdot)$ denote the real and imaginary parts, and α_1 and c_1 are the slope and offset of the constraint line $l_1(j\omega)$. Thus, in words, when taking the real part of the Nyquist curve $Q(\phi, j\omega)$ and multiplying with the slope α_1 and adding the offset c_1, the imaginary part of $Q(\phi, j\omega)$ should be

[§]This only holds when the parameters are unique. In case of repeated parameters, the expression is no longer multilinear.

DOI: 10.1002/rnc

larger to fulfil the constraint. Hence, by rewriting (10), the constraint for the optimization problem can be obtained as

$$-\mathrm{Im}(Q(\phi, j\omega)) + \alpha_1 \mathrm{Re}(Q(\phi, j\omega)) + c_1 < 0, \tag{11}$$

Similarly, the Nyquist curve $Q(\phi, j\omega)$ can be constrained below the line $l_2(j\omega)$ in Figure 4 by setting

$$\mathrm{Im}(Q(\phi, j\omega)) - \alpha_2 \mathrm{Re}(Q(\phi, j\omega)) - c_2 < 0, \tag{12}$$

where α_2 and c_2 are the slope and offset of the constraint line $l_2(j\omega)$.

In (11)–(12), $Q(\phi, j\omega)$ (for stability of the closed-loop system) can be replaced by $Q_\Delta(\phi, j\omega)$ to obtain constraints for closed-loop performance requirements. Hence, when a stabilizing controller is required, one would constrain $Q(\phi, j\omega)$ from encircling the origin. If performance requirements on the closed-loop system are required, one would use $Q_\Delta(\phi, j\omega)$. The constraints imposed to satisfy closed-loop performance (i.e., constraining $Q_\Delta(\phi, j\omega)$) are denoted by $l_\Delta(\phi, j\omega)$.

It should be stressed here that constraints can be assigned per frequency point. Hence, as is indicated in Figure 4, the left part (lower frequencies) of the Nyquist curves (grey) are constrained from above by $l_2(j\omega)$. Similarly, the right part (higher frequencies) of the Nyquist curves (black) are constrained from below by $l_1(j\omega)$. Thus, in this illustrative example, the Nyquist curves have one 'active' constraint per frequency (but is not necessarily limited to one constraint).

Before a feasibility problem can be constructed using $l_\Delta(\phi, j\omega)$, the realization of the performance perturbation Δ_P is discussed in the next subsection.

3.3. Realization of performance Δ_P

In the subsequent paragraphs, some details regarding the realization of the performance perturbation Δ_P are given (also refer to [49, 50]). The performance Δ_P is described by $\|\Delta_P(s)\|_\infty \leqslant 1$ and $\Delta_P \in \mathcal{RH}_\infty^{n_w \times n_z}$. Thus, considering $l_\Delta(\phi, j\omega)$ which consists of $\Delta_P(j\omega)$, this would imply evaluating an infinite number of constraints (i.e., per frequency all realizations of $\Delta_P(j\omega)$ that satisfy $\max_\omega \bar{\sigma}(\Delta_P(j\omega)) \leqslant 1$). To avoid this, the performance $\Delta_P(j\omega)$ is realized by n_d points randomly drawn from $\max_\omega \bar{\sigma}(\Delta_P(j\omega)) \leqslant 1$.

The realization of the performance $\Delta_P(j\omega)$ is denoted by $\bar{\Delta}_P(j\omega)$ and the determinant expression including $\bar{\Delta}_P(j\omega)$ is denoted by $Q_{\bar{\Delta}}(\phi, j\omega)$. It should hold that at every frequency, the Nyquist curve $\bar{\Delta}_P(j\omega)$ should not violate the constraints. Thus, it is sufficient to check only the boundary [51], and therefore, relevant constraints can be obtained by realizing $\Delta_P(j\omega)$ with maximum singular value, that is, $\bar{\sigma}(\Delta_P(j\omega)) = 1$. Hence, the set

$$\bar{\Delta}_{\mathbf{P}} := \{\bar{\Delta}_P \mid \bar{\sigma}\left(\bar{\Delta}_P(j\omega)\right) = 1\}$$

contains the relevant realizations for the constraints. Notice that the number of constraints is proportional to the number n_d of realizations of Δ_P. By choosing the number n_d of realizations sufficiently large, the probability of 'missing' a critical uncertainty can be made small. Also notice that it is sufficient to check the boundary, because of the fact that an LFT will map closed contours in closed contours [52].

Thus, with the realizations $\bar{\Delta}_P(j\omega)$, a feasibility problem can now be constructed such that the controller parameters can be computed.

3.4. Multilinear feasibility problem

Given the frequency response data of the generalized plant $P(j\omega)$, the line constraint(s) $l(\phi, j\omega)$ for stability or $l_{\Delta_P}(\phi, j\omega)$ for performance, and the realizations $\bar{\Delta}_P$ of the performance Δ_P, a feasibility problem can be formulated to obtain stability and performance of the closed-loop system. For this, it should hold that for every frequency the constraints should be satisfied. For stability, the following problem is obtained

$$\text{Find } \phi \text{ such that } \quad l(\phi, j\omega) < 0 \quad \forall \omega \in \mathbf{\Omega}, \tag{13}$$

DOI: 10.1002/rnc

where $\mathbf{\Omega}$ is the finite discrete set containing the frequency grid of the measured plant FRF. For performance, the following problem is obtained

$$\text{Find } \phi \text{ such that } \quad l_{\bar{\Delta}_P}(\phi, j\omega) < 0 \quad \forall \omega \in \mathbf{\Omega},\ \forall \bar{\Delta}_P(j\omega) \in \bar{\Delta}_{\mathbf{P}}. \tag{14}$$

By solving the aforementioned feasibility problems, controller parameters ϕ are obtained for which the closed-loop system is stable in the case of (13) and for which the closed-loop system is stable and satisfies the performance requirements in the case of (14).

Note that in (13) and (14), multiple constraints can be used, for example, such as in Figure 4, which can be assigned per frequency. Further remark that the size of the feasibility problem (13) depends on the number of frequency points, the number of constraints active per frequency, and in the case of (14) also on the number n_d of performance realizations $\bar{\Delta}_P$. Hence, the feasibility problem has N constraints in the former case (13) and $N \cdot n_d$ constraints in the latter case (14), with N the number of frequency points considered. Finally, it is important to note that the number of constraints in the feasibility problems thus does not depend on the number of controller parameters.

3.5. Convex feasibility problem

In the previous sections, it is shown that by extracting the tunable controller parameters into the diagonal form, the resulting feasibility problem is multilinear in the controller parameters ϕ. However, by creating the generalized plant configuration slightly different, the feasibility problem becomes a convex feasibility problem for some special controller cases. To see this, the diagonal controller parameter matrix with the perturbation Δ_P as was previously used in (7), that is,

$$\left[\begin{array}{c|ccc} \Delta_P(j\omega) & \multicolumn{3}{c}{0} \\ \hline & \phi_1 & & 0 \\ 0 & & \ddots & \\ & 0 & & \phi_m \end{array}\right]$$

is modified to

$$K_{\mathrm{I}}(\phi, j\omega) = \left[\begin{array}{cc} \Delta_P(j\omega) & 0 \\ 0 & C_{\mathrm{I}}(\phi, j\omega) \end{array}\right], \tag{15}$$

where $C_{\mathrm{I}}(\phi, j\omega)$ is now the full controller including the tunable controller parameters. To do so, the generalized plant needs to be changed accordingly as well. Thus, instead of extracting the tunable parameters in a diagonal matrix gain K (as was done in Figure 2 and (2)) and absorbing the rest of the controller in the generalized plant, the full controller is included in $C_{\mathrm{I}}(\phi, j\omega)$ (15). In the case that $C_{\mathrm{I}}(\phi, j\omega)$ in (15) is SISO and affine in the tunable controller parameters ϕ, the approach results in a convex feasibility problem. This can be demonstrated by writing down the determinant expression for the SISO controller case and a scalar perturbation block Δ_P. The performance condition then becomes

$$\det\left(I - K_{\mathrm{I}}(\phi, j\omega) P(j\omega)\right). \tag{16}$$

Substituting (15) in (16) gives the determinant expression

$$(1 - \Delta_P P_{11})\,(1 - C_{\mathrm{I}}(\phi) P_{22}) - \Delta_P P_{12} C_{\mathrm{I}}(\phi) P_{21}, \tag{17}$$

which is affine in the controller parameters ϕ. Hence, SISO controllers including, for example, PID controllers (assuming an affine parameterization) result in a convex feasibility problem. Note that the realization of the performance Δ_P can be multidimensional without affecting the procedure as discussed previously for including the line constraints in the Nyquist diagram. Furthermore, also note that in the case of a Multi-Input Single-Output controller with affine parameterization, the problem remains convex, and that in the case of a Single-Input Multi-Output controller, the problem is no longer convex. The derivation of the latter observation is left to the reader.

DOI: 10.1002/rnc

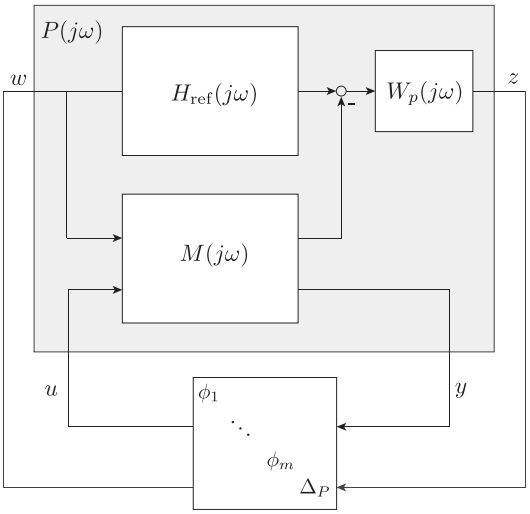

Figure 5. Grey-box system identification configuration.

4. GREY-BOX SYSTEM IDENTIFICATION

The controller design methodology presented in the previous sections fits a controller to the data. In this section, the previously introduced approach is extended to a class of system identification methods. Thus, instead of fitting a controller to the data, a model is fitted to the data. This is achieved by a slight reformulation of the problem, in such a way that the parameters of a parameterized model can be computed. The approach was previously presented in [53] and applied to identify a simplified control-oriented model of the yaw dynamics of a two-bladed wind turbine.

The main approach is in fact a model matching problem posed as an $\mathcal{H}_\infty$ problem [54]. The parameters ϕ of the model $H(j\omega)$, which should be matched to a measured FRF, are extracted into a diagonal form by an LFT, that is, $H(j\omega) = F_l(M(j\omega), \phi)$. Then, consider the schematic block diagram in Figure 5. In this diagram, the measured FRF of a plant is denoted by $H_{\mathrm{ref}}(j\omega)$, and the model $M(jw)$ with tunable model parameters ϕ is obtained by the previously mentioned LFT. The outputs of $M(j\omega)$ are element-wise subtracted from the outputs of the reference model $H_{\mathrm{ref}}(j\omega)$. The output z of the generalized plant $P(j\omega)$ is then given by the differenced outputs, weighted by the performance weight $W_p(j\omega)$. Similarly as before, the full perturbation block Δ_P closes the loop from z to w.

In order to compute the model parameters ϕ such that $H(j\omega)$ is close to $H_{\mathrm{ref}}(j\omega)$, the exact same techniques as in the previous sections can be applied. Again, by constraining the Nyquist curves from encircling or crossing the origin, feasibility problems equal to (13) and (14) are obtained. For feasible solutions of (14) it thus holds that $\|T_{\mathrm{wz}}\|_\infty < 1$.

In the next section, the experimental setup is described, which is used to demonstrate the previously presented methodologies.

5. EXPERIMENTAL SETUP

The experimental setup considered in this paper is a double-mass-spring-damper system, which can be modeled[¶] by Figure 6. A force F acts on the first mass m_1, which is connected through a flexible shaft to the second mass m_2. The positions of the masses are denoted by x_1 and x_2, and the stiffness and damping of the system are denoted by k and d, respectively. A lightly damped system will show

[¶]Note that the experimental setup is rotational, whereas the considered simulation examples are translational. For that reason, the model in Figure 6 is chosen to be translational. Replacing the force input F with a torque T, the masses m_1 and m_2 with inertias J_1 and J_2, and the positions x_1 and x_2 with θ_1 and θ_2, the equivalent rotational model is obtained.

DOI: 10.1002/rnc

a clearly visible resonance peak in a frequency plot. The system can be described by two transfer functions. The transfer function from input F to position x_1 (collocated) is given by

$$\frac{x_1}{F} = \frac{m_1 s^2 + ds + k}{m_1 m_2 s^4 + (m_1 + m_2) d s^3 + (m_1 + m_2) k s^2}, \tag{18}$$

and the transfer function from input F to position x_2 (non-collocated) is given by

$$\frac{x_2}{F} = \frac{ds + k}{m_1 m_2 s^4 + (m_1 + m_2) d s^3 + (m_1 + m_2) k s^2}. \tag{19}$$

The resonance frequency ω_r is at $\omega_r = \sqrt{k/m_r}$, with $m_r = m_1 m_2/(m_1 + m_2)$.

A photograph of the experimental setup is shown in Figure 7. This setup will be used to demonstrate the controller design methodology. The DC motor drives the first mass, which is connected to the second mass through a flexible shaft. Both the first mass and second mass have position encoders. The force actuation commands and position readbacks are connected to a pc using a real-time connection, which is operated from MATLAB Simulink. An FRF of the system is obtained by repeated closed-loop experiments in which the system was excited with white noise. From the closed-loop data, the open-loop response is extracted and subsequently the plant dynamics can be obtained. By averaging the results for each frequency over a number of experiments, an FRF is obtained. The FRF results for both the collocated and the non-collocated system are shown in Figure 8. The resonance frequency ω_r is at approximately 54.2 Hz.

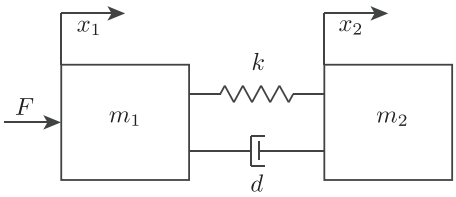

Figure 6. Double mass-spring-damper system.

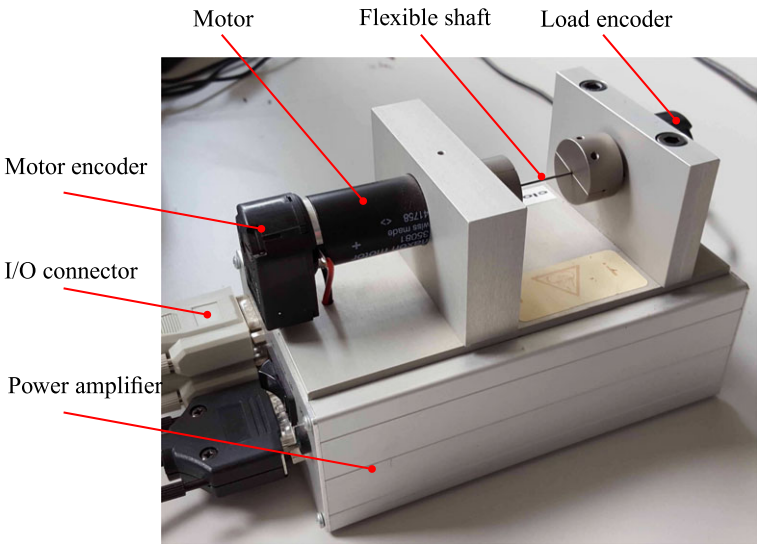

Figure 7. Experimental setup of two masses connected by a flexible shaft. The left mass (only partially visible) is actuated by a DC motor.

DOI: 10.1002/rnc

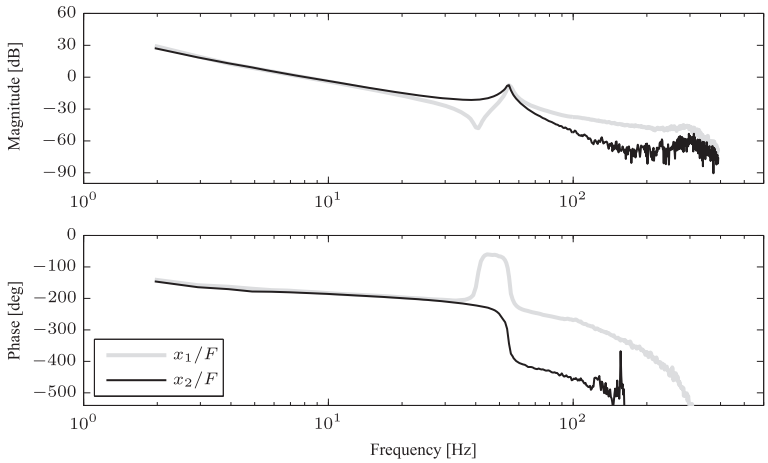

Figure 8. Measured frequency-response function of the experimental setup.

6. RESULTS

In this section, the design methodology presented in Sections 2–4 is applied to two simulation examples and to three example cases using the experimental setup discussed in Section 5. The example cases involve non-collocated control (i.e., the force input F is used to control the position of the second mass m_2) according to [55]. The following five example cases are considered:

1. Computing a PD controller that achieves certain performance requirements on a simulation example;
2. Computing a PD controller and the stiffness parameter of the system (plant/controller optimization) that achieves certain performance requirements on a simulation example;
3. Computing a PD controller *without* notch filter to obtain certain performance specifications on the experimental setup;
4. Computing a PD controller *with* notch filter to obtain certain performance specifications on the experimental setup;
5. Computing the parameters (m_1, m_2, k, d) in (19) using the FRF of the experimental setup and the grey-box system identification method outlined in Section 4.

In all example cases, the dimension of Δ_P is 1×1 (a single input w and a single output z). Therefore, the perturbation Δ_P is realized by drawing n_d samples from the unit circle (i.e., $\|\bar{\Delta}_P\| = 1$). The feasibility problem obtained in each example case is solved by using YALMIP [56] with MATLAB's `fmincon` solver with default settings (the gradients are thus estimated by finite differences).

6.1. Simulation results

For the simulation examples, the model in Figure 6 is used. The simulation examples were previously presented in [39] and are adopted here with minor changes.

6.1.1. PD controller design. In the first simulation example, the input F is used to control the position x_2 of the second mass. A PD controller with negative feedback is used to obtain certain closed-loop specifications. It is assumed that the system has a time delay of $T_d = 0.1\,\mathrm{s}$, which is modeled by a first-order Padé approximation. Hence, the transfer function (19) is connected in series with the time delay approximation and is denoted by $G(s)$. The output of the time-delayed system $G(s)$, $y = x_{2,d}$, is connected to the PD controller given by

$$C_{\mathrm{PD}}(s) = \frac{K_p + K_d s}{0.01s + 1}. \tag{20}$$

DOI: 10.1002/rnc

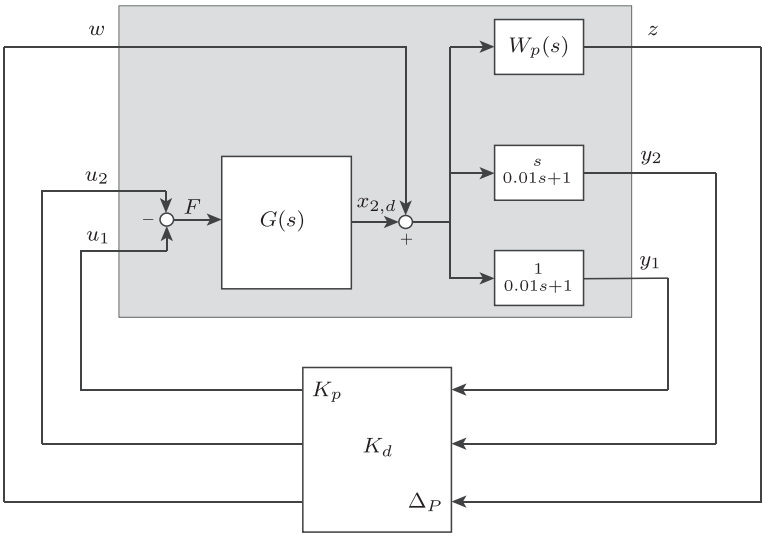

Figure 9. Configuration of the plant and controller for the double-mass-spring damper system. The PD controller is partly absorbed in the generalized plant.

In order to maintain a diagonal control structure with only the controller parameters on the diagonal, the fractions in (20) are absorbed into the plant. Then, closed-loop system performance is imposed by a bound on the sensitivity function by means of a second-order performance weight (refer to [4])

$$W_p(s) = \frac{s^2/M_p^2 + 2\beta_p\omega_B s + \omega_B^2}{s^2 + 2\beta_p A_p\omega_B s + (A_p\omega_B)^2},$$

where $\beta_p = 0.3$, $M_p = 2$, $A_p = 1 \cdot 10^{-3}$ and $\omega_B = 0.1$. The complete generalized plant configuration for this system is shown in Figure 9, where also the complex perturbation Δ_P is included. In this example, the parameter values are taken as $m_1 = m_2 = k = 1$ and $d = 0.05$.

Because the complexity of this problem is relatively low (only two controller parameters need to be found), a grid search of the controller parameters is carried out. For each combination of K_p and K_d, $\|T_{\text{wz}}\|_\infty$ is computed. Thus, the solution space can be visualized and is shown in Figure 10. The lowest obtained $\mathcal{H}_\infty$ norm by the grid search is $\|T_{\text{wz}}\|_\infty = 0.884$, which is obtained for $K_p = 0.068$ and $K_d = 0.142$. For comparison, the method in [32] by using the frequency-domain robust control toolbox (FDRCT) [57] is also used. As mentioned in the introduction, this method requires a desired open-loop transfer function $L_d(s)$. Setting $L_d(s) = W_p - 1$ (as suggested in [57]) gives a satisfactorily result for which $\|T_{\text{wz}}\|_\infty = 0.861$, $K_p = 0.069$, and $K_d = 0.145$.

In order to compute controller parameters that yield performance, the feasibility problem in (14) is constructed. Because the generalized plant is stable, the Nyquist curve should not encircle the origin. A basic outline of the Nyquist curve was obtained (similar to Figure 4) from the general system properties. With this knowledge and for $N = 400$ frequency points on a logarithmic scale in the interval $[0.1, 10]$ rad/s, two constraints in the Nyquist diagram are formulated, that is,

$$\begin{aligned} \text{Im}(Q_\Delta(j\omega)) + 0.2\text{Re}(Q_\Delta(j\omega)) - 0.001 < 0 \quad &\text{for } \omega \leqslant 0.16, \\ -\text{Im}(Q_\Delta(j\omega)) - 5\text{Re}(Q_\Delta(j\omega)) + 0.001 < 0 \quad &\text{for } \omega \geqslant 0.20. \end{aligned}$$

The performance $\Delta_P(j\omega)$ is for each ω realized by n_d points randomly sampled on the unit circle using a uniform distribution. Finally, the feasibility problem is solved by using [56] and MATLAB's `fmincon` function. The optimization procedure is carried out for 100 Monte Carlo simulations, where for each simulation a new realization of the perturbation Δ_P is computed and the initial controller parameters are uniformly drawn from $[0, 1]$ so as to be able to evaluate convergence.

The obtained results for varying number n_d are listed in Table I, which for reference also lists the

DOI: 10.1002/rnc

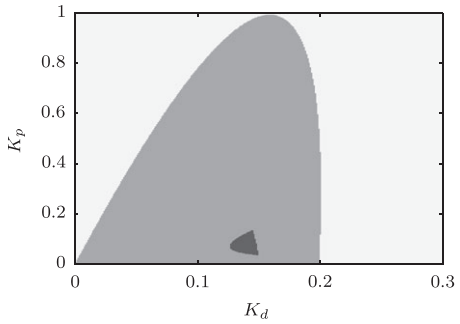

Figure 10. Results of the grid search of K_p and K_d for the controlled double-mass-spring-damper system. The light grey area represents controller parameter combinations resulting in an unstable closed-loop system, the grey area represents combinations that yield a stable closed-loop system, and the dark grey area represents the solutions with $\mathcal{H}_\infty$-norm lower than 1.

Table I. Optimization results of the first simulation example.

Description	$\mathcal{H}_\infty^{\min}$	$\mathcal{H}_\infty^{\max}$	Success [%]
Grid search	0.884	–	–
FDRCT	0.861	–	–
Nyquist optim. ($n_d = 5$)	0.900	2.884	46
Nyquist optim. ($n_d = 10$)	0.913	2.403	55
Nyquist optim. ($n_d = 25$)	0.892	1.072	86
Nyquist optim. ($n_d = 50$)	0.930	1.058	98
Nyquist optim. ($n_d = 100$)	0.913	0.988	100

'Success' indicates the percentage of solutions that satisfy the performance condition.

grid search result and the FDRCT result. It should be stressed that the proposed methodology does not minimize the $\mathcal{H}_\infty$-norm, but rather tries to find a feasible solution[‖] for which it is then known that $\|T_{\text{wz}}\|_\infty < 1$. From Table I, it can also be seen that for increasing n_d, the number of solutions that satisfy the performance condition. Moreover, for $n_d = 100$ realizations of Δ_P all trials satisfied the performance condition. The reason for not obtaining the lowest norm (i.e., the FDRCT result) is twofold. First, the optimization solver quits when a feasible solution is found rather than minimizing $\|T_{\text{wz}}\|_\infty$. Second, it is possible that the constraint lines were chosen too conservative and therefore constrained from solutions that yield the lowest norm. The Nyquist curve of the plant with controller, obtained for the case with $n_d = 100$ with lowest $\mathcal{H}_\infty$ norm ($\|T_{\text{wz}}\|_\infty = 0.913$, $K_p = 0.048$, and $K_d = 0.1474$), is shown in Figure 11. The graph is plotted for a densely (large n_d) realized complex perturbation Δ_P, from which it can be observed that the origin (indicated by $+$) is not encircled.

6.1.2. Simultaneous plant/control design. In the second simulation example, the simultaneous design of controller and plant parameters is considered. The goal of this example is to find PD controller parameters and the value of the stiffness parameter of the system such that a closed-loop performance specification is satisfied. The stiffness parameter k in Figure 6 is extracted from the model by adding an external force F_k, which acts on both masses (Figure 12). The dynamics for the modified system $G_1(s)$ are given by

$$\begin{bmatrix} x_1 \\ x_2 \end{bmatrix} = G_1(s) \begin{bmatrix} F \\ F_k \end{bmatrix},$$

[‖]The $\mathcal{H}_\infty$ norm can, however, be minimized by including, for example, a bisection algorithm.

DOI: 10.1002/rnc

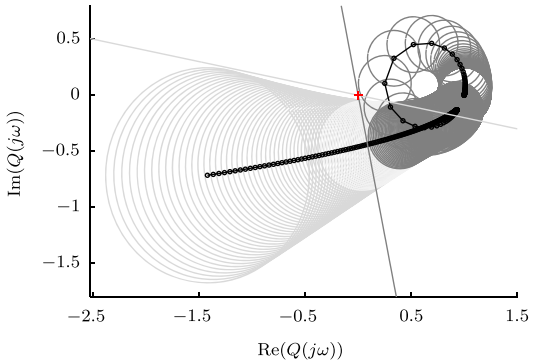

Figure 11. Resulting Nyquist plots of $Q(\phi, j\omega)$ (black) and $Q_\Delta(\phi, j\omega)$ (light grey and dark grey) for the first simulation example. The colors of the constraint lines and the Nyquist curve are matched to indicate where they hold.

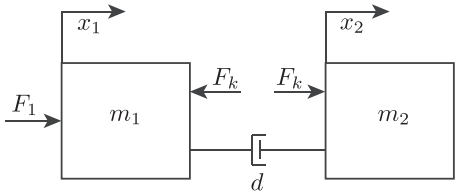

Figure 12. Example case 2: double-mass-damper with additional external force input F_k.

with $G_1(s)$ equal to

$$\frac{1}{m_1 m_2 s^3 + (m_1 + m_2) d s^2} \begin{bmatrix} m_2 s + d & -m_2 s \\ d & m_1 s \end{bmatrix}.$$

Note that by taking

$$F_k = \kappa(x_1 - x_2), \tag{21}$$

and setting $\kappa = k$, the systems in Figures 6 and 12 are identical. If F_k is chosen as in (21), it can be regarded as adding stiffness to the system. Thus, by absorbing $x_1 - x_2$ into the plant, κ becomes a structural parameter that can be optimized. Finally, the positions x_1 and x_2 are assumed to have a time delay of 0.05 s, modeled by a first-order Padé approximation, and are denoted by $x_{1,d}$ and $x_{2,d}$.

As with the previous case, a PD controller is used to obtain certain closed-loop specifications. In order to avoid trivial solutions (e.g., κ going to infinity), the performance weight $W_p(s)$ of the previous case is modified to

$$W_{p,1}(s) = W_p(s) \times \frac{s^2 + 2\beta_p^* A_p^* \omega_B^* s + (A_p^* \omega_B^*)^2}{s^2/(M_p^*)^2 + 2\beta_p^* \omega_B^* s + (\omega_B^*)^2},$$

where $\beta_p^* = 0.7$, $M_p^* = 1.9$, $A_p^* = 0.9$ and $\omega_B^* = 1$. The modification can be regarded as putting a constraint on the resonance frequency of the system. With the modified performance weight $W_{p,1}(s)$, the generalized plant is then depicted in Figure 13. Similar to the previous case, a grid search of the three controller parameters is carried out in order to visualize the solution space. The results are shown in Figure 14.

Now the proposed method is applied to find the controller parameters K_p and K_d, and the structural parameter κ, such that the performance condition (7) is satisfied. The performance $\Delta_P(j\omega)$ is realized by $n_d = 100$ points randomly sampled on the unit circle and the following constraints are applied

DOI: 10.1002/rnc

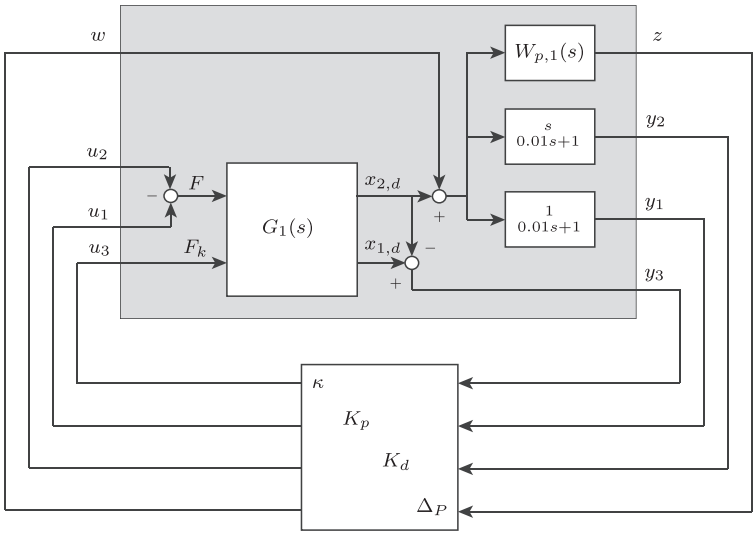

Figure 13. Configuration of the plant and controller for the simultaneous design of plant and controller.

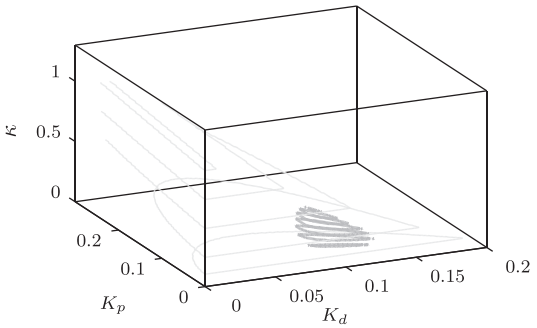

Figure 14. Results of the grid search of K_p, K_d, and κ for the double-mass-damper system. The volume within the light grey contour lines indicate the parameter combinations resulting in a stable closed-loop system and the volume within the dark grey contour lines are combinations that yield a stable closed-loop system with $\mathcal{H}_\infty$ norm lower than 1.

$$-\mathrm{Im}(Q_\Delta(j\omega)) + 0.7\mathrm{Re}(Q_\Delta(j\omega)) + 0.001 < 0 \quad \text{for } \omega \leqslant 0.37,$$
$$\mathrm{Im}(Q_\Delta(j\omega)) + 0.001 < 0 \quad \text{for } 0.54 \leqslant \omega \leqslant 0.57.$$

Then, 100 Monte Carlo simulations for uniformly drawn initial parameter values in the interval $[0, 1]$ were performed. The solution with the lowest $\mathcal{H}_\infty$ has controller parameters $K_p = 0.0534$, $K_d = 0.1088$, $\kappa = 0.1604$, and $\|T_{\mathrm{wz}}\|_\infty = 0.862$. This is close to optimal, because with a grid search the lowest $\mathcal{H}_\infty$ norm was found to be 0.8587.

6.2. *Experimental results*

In the experimental results, the experimental setup of Section 5 is used to demonstrate the controller design and grey-box system identification methods. The FRF as shown in Figure 8 is used to design the controllers, with 400 linearly spaced frequency points in the interval $[1.95, 391.6]$ Hz.

6.2.1. PD controller. In the first case, the objective is to find the proportional and derivative gain of a PD controller such that certain frequency-domain performance specifications are met. The

DOI: 10.1002/rnc

controller structure is given by

$$C_{\mathrm{PD},1}(s) = \frac{K_p + K_d s}{1/(2\pi f_c)s + 1}, \tag{22}$$

where $f_c = 120\,\mathrm{Hz}$ is the cut-off frequency of the low-pass filter and (K_p, K_d) are the controller parameters that are sought. The performance requirement of the controlled system is a closed-loop bandwidth of 3 Hz. To satisfy this, the following second-order performance weight [4] is used

$$W_{p,2}(s) = \frac{s^2/M_p^2 + 2\beta_p\omega_B s + \omega_B^2}{s^2 + 2\beta_p A_p\omega_B s + (A_p\omega_B)^2}, \tag{23}$$

with $\beta_p = 0.8$, a maximum sensitivity function gain of 6 dB by setting $M_p = 1.4$, $A_p = 0.05$, and a desired bandwidth of $\omega_B = 2\pi 2.8$ rad/s. The generalized plant configuration is therefore similar to Figure 9.

It is found during the experiments that the proportional gain K_p greatly influenced the reference tracking performance. A low value of K_p results in poor reference tracking, whereas a larger value of K_p gives satisfactory reference tracking performance, because friction effects are (partly) overcome. Hence, in order to have satisfactory tracking performance, the proportional gain K_p was maximized during the optimization process (in this case, the derivative gain is more dominant for the bandwidth of the system). Therefore, the feasibility problem (14) was turned into an optimization problem by maximizing the proportional gain K_p subject to the constraints (14). For the optimization problem, the perturbation block Δ_P was realized by $n_d = 100$ points on the unit circle and two line constraints were used. The gains of the final implemented controller are $K_p = 0.1234$ and $K_d = 0.0091$, for which the $\mathcal{H}_\infty$ norm is 0.950. The resulting sensitivity function and the inverse of the performance weight are shown in Figure 15, from which it can be seen that the sensitivity function remains below the inverse of the performance weight.

The results of the implemented controller on the setup are shown in Figures 16–17. The measured open-loop function of the setup is shown in Figure 16. It can be observed that the cross-over frequency of the loop gain crosses 0 dB around 4 Hz. Moreover, the step response shows decent tracking behavior. The small oscillation in the step response is caused by the resonance of the system.

6.2.2. PD controller with notch filter. For the second controller case, the objective is to increase the bandwidth of the system. To this end, the previous controller (22) is extended with a notch filter,

$$C_{\mathrm{PD},2}(s) = C_{\mathrm{PD},1}(s) \times \frac{s^2 + 2\beta_z\omega_r s + \omega_r^2}{s^2 + 2\beta_p\omega_r s + \omega_r^2}, \tag{24}$$

where ω_r is the resonance frequency of the experimental setup and, β_z and β_p determine the width and deepness of the notch filter. The low-pass filter remains unchanged. Therefore, the generalized plant configuration in Figure 13 is modified to include an LFT of the notch filter. The bandwidth

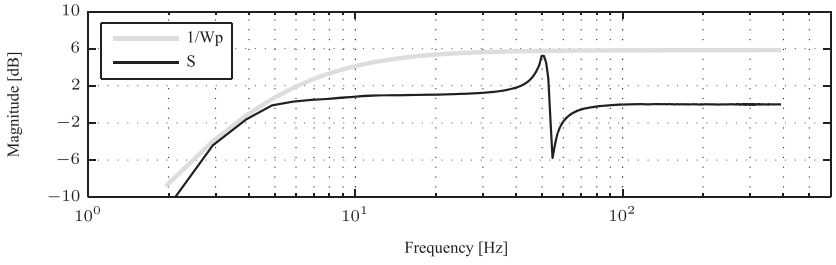

Figure 15. Sensitivity function obtained with the optimized controller for the first experiment (non-collocated PD controller without notch filter). The inverse of the performance weight W_p is also shown.

DOI: 10.1002/rnc

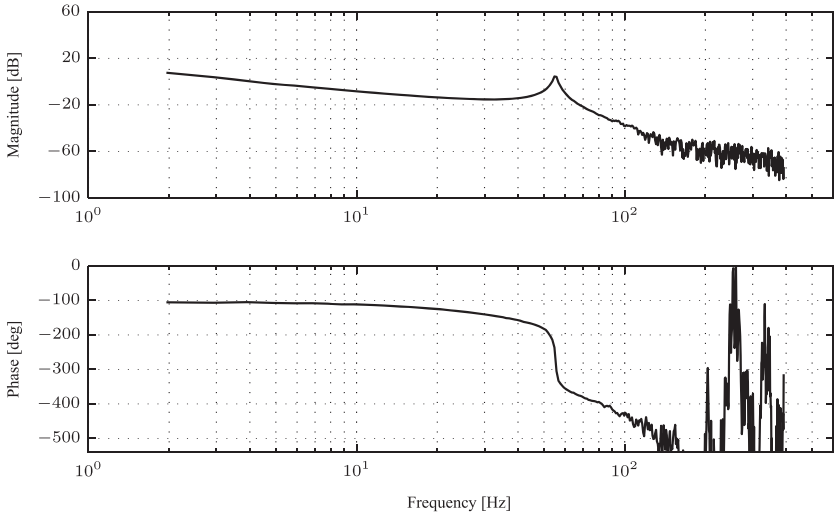

Figure 16. Measured open-loop transfer function of the first experiment (non-collocated PD controller without notch filter).

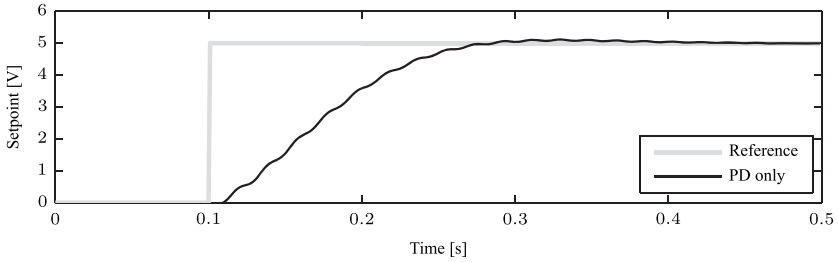

Figure 17. Measured step response of the first experiment (non-collocated PD controller without notch filter).

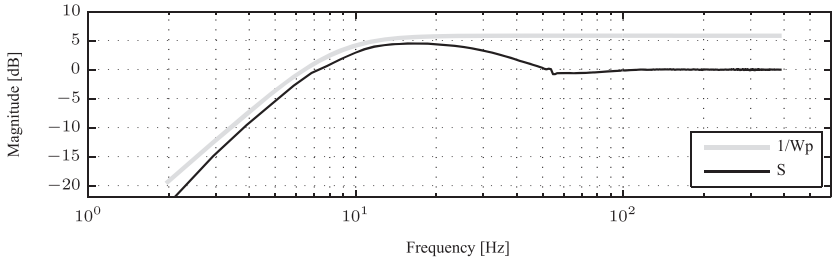

Figure 18. Sensitivity function obtained with the optimized controller for the second experiment (non-collocated PD controller with notch filter). The inverse of the performance weight W_p is also shown.

of the performance weight $W_{p,2}(s)$ in (23) is changed from $\omega_B = 2\pi 2.8$ rad/s to $\omega_B = 2\pi 6$ rad/s. Thus, in this experiment, the controller parameters $(K_p, K_d, \beta_z, \beta_p)$ are sought, such that the modified performance specification is satisfied. Similar to the previous case, four line constraints were used, $n_d = 50$, and an optimization problem maximizing the value of K_p subject to the constraints was solved. The final obtained solution has gain $K_p = 0.6210$, $K_d = 0.0216$, $\beta_z = 0.0406$, and $\beta_p = 0.5190$. For these gains, the $\mathcal{H}_\infty$ norm of the weighted closed-loop system is 0.8989. For this controller, the sensitivity function and inverse of the performance weight are shown in Figure 18.

The results of the PD controller augmented with notch filter are shown in Figures 19–20. From the measured loop gain of the system it can be observed that the 0 dB line is now crossed at a frequency of roughly 10 Hz. With respect to the previous case, the bandwidth has increased by 2.5 times. The

DOI: 10.1002/rnc

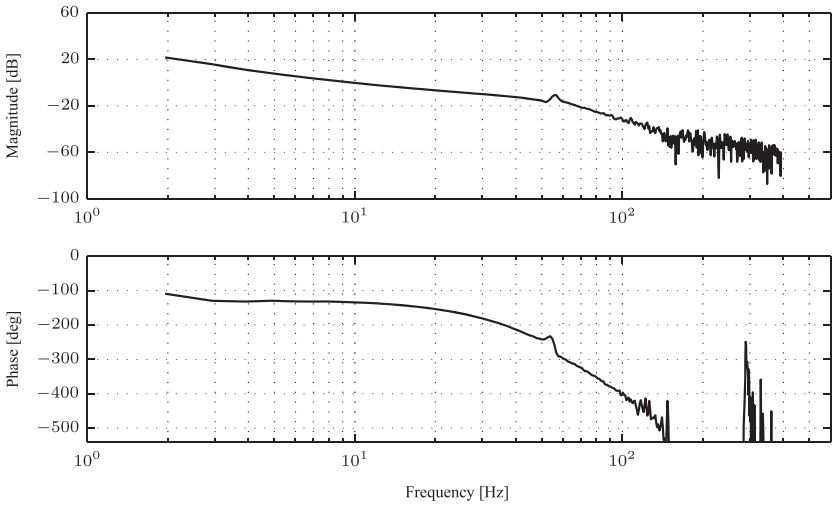

Figure 19. Measured open-loop transfer function of the second experiment (non-collocated PD controller with notch filter).

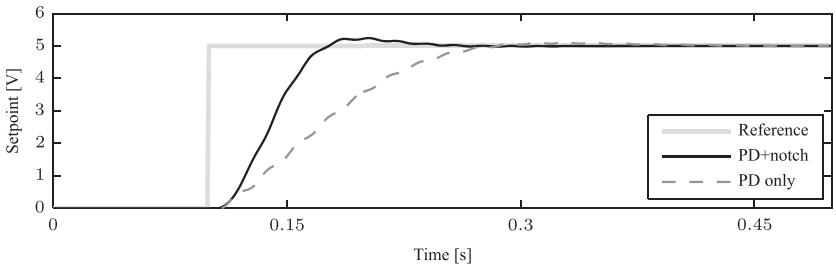

Figure 20. Measured step response of the second experiment (non-collocated PD controller with notch filter). The measured step response of the first experiment is also shown.

increased bandwidth can also be observed from the step response where both controller cases are compared.

6.2.3. Grey-box system identification. In the final case study, the grey-box system identification method introduced in Section 4 is applied to obtain model parameters. For many motion systems, that is, mechanical structures, the damping is typically fairly low and can be considered linear. In fact, it can often be considered as proportional, which is an even stronger assumption. This has been experimentally investigated in, for example, [58] and [59], where dedicated frequency response based tests are used to quantify the nonlinearities. These approaches are well supported by theoretical considerations, see, for example, [2]. Based on the latter studies and observations thereof, it is justified that (19) can be used to model the dynamics of the experimental setup.

For this purpose, the generalized plant structure as shown in Figure 5 is used. The model $M(s)$ is obtained by an LFT of the transfer function in (19), that is, the parameters (m_1, m_2, k, d) are extracted from the transfer function such that they can be put in the diagonal form used throughout this paper. From the step responses obtained earlier, a small time delay (approximately 0.005 s) can be observed, which was modeled by a first-order Padé approximation. Selecting the performance weight for this example case is not trivial. However, it was found that multiplying with the inverse of the plant FRF and an inverted notch filter at the resonance frequency of the system gave a satisfactory result. The performance weight is thus given by

$$W_{p,3}(j\omega) = \frac{1}{H_{\text{ref}}(j\omega)} \times \frac{10j\omega}{(j\omega)^2 + 2\omega_r 0.01 j\omega + \omega_r^2}.$$

DOI: 10.1002/rnc

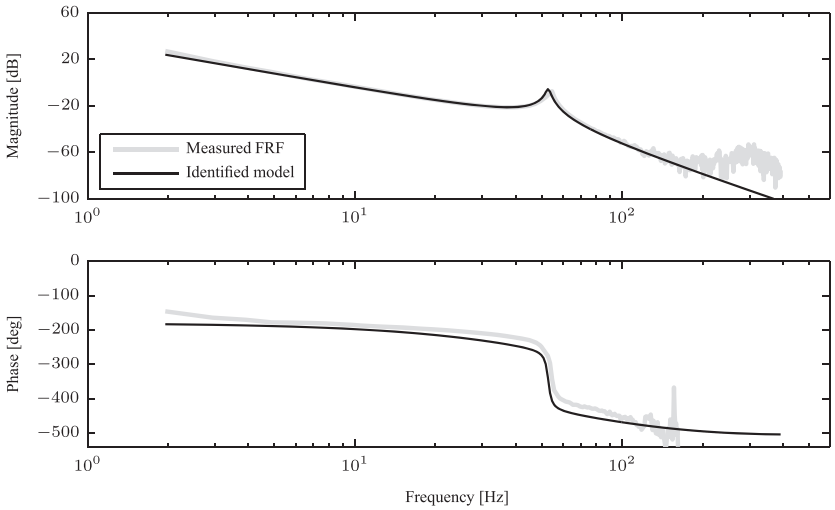

Figure 21. Grey-box system identified model.

It was also found that two constraint lines are required to constrain the Nyquist curve from crossing zero. The feasibility problem was then solved by constraining $m_1 = m_2$ (the masses are assumed to be of equal weight) and d to be smaller than 0.01, and $n_d = 25$. Note that setting $m_1 = m_2$ has the consequence that quadratic terms appear in the feasibility problem. The feasible solution with the lowest $\mathcal{H}_\infty$ norm, that is, $\|T_{\text{wz}}\|_\infty = 0.5151$, is shown in Figure 21. For this solution, the parameters are $m_1 = 0.0048$, $m_2 = 0.0048$, $k = 11.4494$, and $d = 0.0014$.

7. CONCLUSION

A novel frequency-domain design methodology exploiting the generalized Nyquist stability criterion is presented. The methodology focuses mainly on fixed-structure controllers, of which the tunable parameters can be extracted into a diagonal form. By introducing line constraints in the Nyquist diagram, the Nyquist curve is prevented from encircling or crossing the origin, such that stability and certain performance specifications of the closed-loop system can be achieved. The line constraints typically result in a feasibility problem multilinear in the tunable controller parameters. However, it was shown that in special controller cases, the feasibility problem becomes convex in the tunable parameters. The methodology can directly be applied to design fixed-structure controllers using a measured FRF of the plant, but can also be used to simultaneously optimize plant and controller parameters, and for grey-box system identification. The method has been successfully demonstrated through simulation examples and on an experimental setup. Future research is directed towards techniques that simplify the selection of the constraint lines, which will enhance the proposed methodology.

ACKNOWLEDGEMENTS

The work in this paper is funded and supported by the Far and Large Offshore Wind (FLOW) program, no. 91071, *Integrated design of far large offshore wind turbines*, by the NWO Veni Grant, no. 11930, *Reconfigurable Floating Wind Farms*, and by the Innovational Research Incentives Scheme under the VENI grant Precision Motion: Beyond the Nanometer (no. 13073) awarded by NWO (The Netherlands Organisation for Scientific Research) and STW (Dutch Science Foundation).

REFERENCES

1. van der Veen GJ, van Wingerden JW, Fleming PA, Scholbrock AK, Verhaegen M. Global data-driven modeling of wind turbines in the presence of turbulence. *Control Engineering Practice* 2013; **21**(4):441–454.
2. Pintelon R, Schoukens J. *System Identification: A Frequency Domain Approach*. Wiley: Hoboken, New Jersey, 2012.

DOI: 10.1002/rnc

3. Zhou K, Doyle JC, Glover K. *Robust and Optimal Control*. Prentice Hall: Upper Saddle River, New Jersey, 1996.
4. Skogestad S, Postlethwaite I. *Multivariable Feedback Control: Analysis and Design*. John Wiley & Sons: Chicester, 2006.
5. Doyle JC, Glover K, Khargonekar PP, Francis BA. State-space solutions to standard $\mathcal{H}_2$ and $\mathcal{H}_\infty$; control problems. *IEEE Transactions on Automatic Control* 1989; **34**(8):831–847.
6. Gahinet P, Apkarian P. A linear matrix inequality approach to $\mathcal{H}_\infty$ Control. *International Journal of Robust and Nonlinear Control* 1994; **4**:421–448.
7. Iwasaki T, Skelton RE. All controllers for the general $\mathcal{H}_\infty$ control problem: LMI existence conditions and state space formulas. *Automatica* 1994; **30**(8):1307–1317.
8. Nemirovskii A. Several NP-hard problems arising in robust stability analysis. *Mathematics of Control, Signals and Systems* 1993; **6**(2):99–105.
9. Blondel V, Tsitsiklis JN. NP-hardness of some linear control design problems. *SIAM Journal on Control and Optimization* 1997; **35**(6):2118–2127.
10. Rotkowitz M, Lall S. A characterization of convex problems in decentralized control. *IEEE Transactions on Automatic Control* 2006; **51**(2):274–286.
11. Han J, Skelton RE. An LMI optimization approach for structured linear controllers. *Proceedings of the 42nd IEEE Conference on Decision and control, 2003*, Vol. 5, Maui, Hawaii, USA, 2003; 5143–5148.
12. Karimi A, Khatibi H, Longchamp R. Robust control of polytopic systems by convex optimization. *Automatica* 2007; **43**(8):1395–1402.
13. Scherer CW. Structured $\mathcal{H}_\infty$ optimal control for nested interconnections: a state-space solution. *Systems & Control Letters* 2013; **62**(12):1105–1113.
14. Rubió-Massegú J, Rossell JM, Karimi HR, Palacios-Quiñonero F. Static output-feedback control under information structure constraints. *Automatica* 2013; **49**(1):313–316.
15. Hol CWJ, Scherer CW. *A Sum-of-Squares Approach to Fixed-Order $\mathcal{H}_\infty$ Synthesis*, Lecture Notes in Control and Information Science, 312. Springer, 2005.
16. Henrion D, Sebek M, Kucera V. Positive polynomials and robust stabilization with fixed-order controllers. *IEEE Transactions on Automatic Control* 2003; **48**(7):1178–1186.
17. Popov A, Werner H. Efficient design of low-order $\mathcal{H}_\infty$ optimal controllers using evolutionary algorithms and a bisection approach. *Computer Aided Control System Design, 2006 IEEE International Conference on Control Applications, 2006 IEEE International Symposium on Intelligent Control, 2006*: IEEE, Munich, Germany, 2006; 760–765.
18. Hast M, Åström KJ, Bernhardsson B, Boyd SP. PID design by convex-concave procedure. *2013 European Control Conference*, Zurich, Switzerland, 2013.
19. Maruta I, Kim TH, Sugie T. Fixed-structure controller synthesis: a meta-heuristic approach using simple constrained particle swarm optimization. *Automatica* 2009; **45**(2):553–559.
20. Maruta I, Kim T-H, Song D, Sugie T. Synthesis of fixed-structure robust controllers using a constrained particle swarm optimizer with cyclic neighborhood topology. *Expert Systems with Applications* 2013; **40**(9):3595–3605.
21. Dvijotham K, Todorov E, Fazel M. Convex structured controller design in finite horizon. *IEEE Transactions on Control of Network Systems* 2014; **PP**(99):1–1.
22. Khatibi H, Karimi A. $\mathcal{H}_\infty$ Controller design using an alternative to Youla parameterization. *IEEE Transactions on Automatic Control* 2010; **55**(9):2119–2123.
23. Apkarian P, Noll D. Nonsmooth $\mathcal{H}_\infty$ synthesis. *IEEE Transactions on Automatic Control* 2006; **51**(1):71–86.
24. Apkarian P, Noll D, Rondepierre A. Mixed $\mathcal{H}_2/\mathcal{H}_\infty$ control via nonsmooth optimization. *SIAM Journal on Control and Optimization* 2008; **47**(3):1516–1546.
25. Gahinet P, Apkarian P. Decentralized and fixed-structure $\mathcal{H}_\infty$ control in MATLAB. *2011 50th IEEE Conference on Decision and Control and European Control Conference (CDC-ECC)*, Orlando, Florida, USA, 2011; 8205–8210.
26. Gahinet P, Apkarian P. Structured $\mathcal{H}_\infty$ synthesis in MATLAB. *International Federation of Automatic Control*, Milano, Italy, 2011; 1435–1440.
27. den Hamer AJ, Weiland S, Steinbuch M. Model-free norm-based fixed structure controller synthesis. *Proceedings of the 48th IEEE Conference on Decision and Control, 2009 held jointly with the 2009 28th Chinese Control Conference. CDC/CCC 2009*, Shanghai, China, 2009; 4030–4035.
28. Khadraoui S, Nounou H, Nounou M, Datta A, Bhattacharyya SP. Robust control design method for uncertain system using a set of measurements. *American Control Conference (ACC), 2013*, Washington, DC, USA, 2013; 4325–4330.
29. Parastvand H, Khosrowjerdi M-J. Controller synthesis free of analytical model: fixed-order controllers. *International Journal of Systems Science* 2015; **46**(7):1208–1221.
30. Keel LH, Bhattacharyya SP. Controller synthesis free of analytical models: three term controllers. *IEEE Transactions on Automatic Control* 2008; **53**(6):1353–1369.
31. Galdos K, Karimi A, Longchamp R. $\mathcal{H}_\infty$ Controller design for spectral MIMO models by convex optimization. *Journal of Process Control* 2010; **20**(10):1175–1182.
32. Karimi A, Galdos G. Fixed-order $\boldsymbol{H}_\infty$ controller design for nonparametric models by convex optimization. *Automatica* 2010; **46**(8):1388–1394.
33. Lu J, Skelton RE. Integrating structure and control design to achieve mixed $\mathcal{H}_2/\mathcal{H}_\infty$ performance. *International Journal of Control* 2000; **73**(16):1449–1462.
34. Camino JF, de Oliveira MC, Skelton RE. "Convexifying" linear matrix inequality methods for integrating structure and control design. *Journal of Structural Engineering* 2003; **129**(7):978–988.

DOI: 10.1002/rnc

35. Hiramoto K, Grigoriadis K. Integrated design of structural and control systems with a homotopy like iterative method. *Proceedings of the 2005 American Control Conference, 2005*, Vol. 4, Portland, Oregon, USA, 2005; 2510–2515.
36. Pang CK, Hong F, Wang X. Integrated servo-mechanical control systems design using nyquist plots for high-performance mechatronics. *Microsystem Technologies* 2012; **18**(9-10):1719–1729.
37. van der Veen G, Langelaar M, Keulen F. Integrated topology and controller optimization of motion systems in the frequency domain. *Structural and Multidisciplinary Optimization* 2014:1–13.
38. van Herpen R, Oomen T, Kikken E, van de Wal M, Aangenent W, Steinbuch M. Exploiting additional actuators and sensors for nano-positioning robust motion control. *Mechatronics* 2014; **24**(6):619–631. Control of High-Precision Motion Systems.
39. van Solingen E, van Wingerden JW, De Breuker R, Verhaegen M. Optimization of linear parameterizable $\mathcal{H}_\infty$ controllers in the frequency domain. *19th IFAC World Congress*, Cape Town, South Africa, 2014.
40. van Solingen E, van Wingerden JW. Fixed-structure $\mathcal{H}_\infty$ control design for linear individual pitch control of two-bladed wind turbines. *American Control Conference (ACC), 2014*, Portland, Oregon, USA, 2014.
41. Redheffer RM. On a certain linear fractional transformation. *Journal of Mathematics and Physics* 1960; **39**:269–286.
42. Zhou K, Doyle JC. *Essentials of Robust Control*. Prentice Hall International: Upper Saddle River, New Jersey, 1998.
43. Heuberger PSC, van den Hof PMJ, Wahlberg B. *Modelling and Identification with Rational Orthogonal Basis Functions*. Springer: London, 2005.
44. Karimi A, Zhu Y. Robust $\mathcal{H}_\infty$ controller design using frequency-domain data. *19th IFAC World Congress*, Cape Town, South Africa, 2014.
45. MacFarlane AGJ, Postlethwaite I. The generalized Nyquist stability criterion and multivariable root loci. *International Journal of Control* 1977; **25**(1):81–127.
46. Oomen T, van der Maas R, Rojas CR, Hjalmarsson H. Iterative data-driven $\mathcal{H}_\infty$ norm estimation of multivariable systems with application to robust active vibration isolation. *IEEE Transactions on Control Systems Technology* 2014; **22**(6):2247–2260.
47. Polak E, Mayne DQ, Stimler DM. Control system design via semi-infinite optimization: a review. *Proceedings of the IEEE* 1984; **72**(12):1777–1794.
48. Safonov M, Wyetzner G. Computer-aided stability analysis renders Popov criterion obsolete. *IEEE Transactions on Automatic Control* 1987; **32**(12):1128–1131.
49. Calafiore G, Dabbene F, Tempo R. A survey of randomized algorithms for control synthesis and performance verification. *Journal of Complexity* 2007; **23**(3):301–316.
50. Campi MC. Why is resorting to fate wise? A critical look at randomized algorithms in systems and control. *European Journal of Control* 2010; **16**(5):419–430.
51. Jonckheere EA. *Algebraic and differential topology of robust stability*. Oxford University Press: New York, New York, 1997.
52. Douma SG, van den Hof PMJ. Relations between uncertainty structures in identification for robust control. *Automatica* 2005; **41**(3):439–457. Data-based modelling and system identification.
53. van Solingen E, van Wingerden JW, Beerens J. Integrated yaw design of a downwind two-bladed wind turbine. *American Control Conference (ACC), 2015*, Chicago, Illinois, USA, 2015; 3702–3707. to appear.
54. de Callafon RA, Van den Hof P MJ. Control relevant identification for $\mathcal{H}_\infty$-norm based performance specifications. *Proceedings of the 34th IEEE Conference on Decision and control, 1995*, Vol. 4, New Orleans, Louisiana, USA, 1995; 3498–3503.
55. Wie B, Bernstein DS. Benchmark problems for robust control design. *Journal of Guidance, Control, and Dynamics* 1992; **15**(5):1057–1059.
56. Löfberg J. YALMIP : A toolbox for modeling and optimization in MATLAB. *Proceedings of the CACSD Conference*, Taipei, Taiwan, 2004.
57. Karimi A. Frequency-domain robust control toolbox. *2013 IEEE 52nd Annual Conference on Decision and Control (CDC)*, Florence, Italy, 2013; 3744–3749.
58. Voorhoeve R, van Rietschoten A, Geerardyn E, Oomen T. Identification of high-tech motion systems: an active vibration isolation benchmark. *17th IFAC Symposium on System Identification* Beijing, China, 2015; **48**(28): 1250–1255.
59. Oomen T, van Herpen R, Quist S, van de Wal M, Bosgra O, Steinbuch M. Connecting system identification and robust control for next-generation motion control of a wafer stage. *IEEE Transactions on Control Systems Technology* 2014; **22**(1):102–118.

DOI: 10.1002/rnc